Mon. Not. R. Astron. Soc. **000**, 000–000 (0000) Printed 26 November 2012 (MN LATEX style file v2.2)

Absolute parameters of AE For – a highly active detached binary of late K type⋆

M. Rozyczka,[1]† P. Pietrukowicz,[2] J. Kaluzny,[1] W. Pych[1], R. Angeloni[3,4] and I. Dékány[4,5]

[1] *Nicolaus Copernicus Astronomical Center, Bartycka 18, 00-716 Warszawa, Poland*
[2] *Warsaw University Observatory, Al. Ujazdowskie 4, 00-478 Warszawa, Poland*
[3] *Dept. of Electrical Engineering, Center for Astro-Engineering, Pontificia Universidad Católica de Chile, Av. Vicuña Mackenna 4860, Macul, Santiago, Chile*
[4] *Dept. de Astronomía y Astrofísica, Pontificia Universidad Católica de Chile, Av. Vicuña Mackenna 4860, Macul, Santiago, Chile*
[5] *The Milky Way Millennium Nucleus, Av. Vicuña Mackenna 4860, Macul, Santiago, Chile*

Accepted ... Received ... in original form ...

ABSTRACT

We present photometric and spectroscopic analysis of AE For – a detached eclipsing binary composed of two late K dwarfs. The masses of the components are found to be 0.6314±0.0035 and 0.6197±0.0034 $M_{\odot}$ and the radii to be 0.67±0.03 and 0.63±0.03 $R_{\odot}$ for primary and secondary component, respectively. Both components are significantly oversized compared to theoretical models, which we attribute to their high activity. They show H_{α}, H_{β}, H_{γ}, Ca H and Ca K in emission, and are heavily spotted, causing large variations of the light curve.

Key words: stars: individual: AE For – binaries: eclipsing – stars: fundamental parameters – stars: activity.

1 INTRODUCTION

The 10th magnitude star AE For (CD -25 1273; HIP 14568) was first classified by Stephenson (1986) as a K4 dwarf. In the Hipparcos catalogue (ESA 1997) it was listed as a new eclipsing variable of Algol type with a period of 0.918235(8) d, and a parallax of 32.10±1.78 mas. The latter was revised in 2007 to the presently adopted 31.8±1.96 mas (van Leeuwen 2007), corresponding to 31.5±1.9 pc.

Gizis, Reid & Hawley (2002) found the star to be a double-lined binary with Balmer lines in emission. Emission in Balmer and Ca II H & K lines was also observed by Gray et al. (2006), who estimated the spectral type of AE For at K9 Ve, and classified it as a very active system. A slightly earlier spectral type (K7 Ve) was assigned to AE For by Torres et al. (2006), who also noted its high activity. According to Zasche, Svoboda & Uhlář (2012; hereafter ZSU), the system contains a brown dwarf with a minimal mass of ∼47 M_{Jup} on an eccentric orbit of ∼7 years.

In the solar neighborhood about 7 per cent of detached eclipsing binaries are X-ray emitters (Szczygieł et al. 2008). With its $L_X = 9.4 \times 10^{29}$ erg s^{-1} (Huensch et al. 1999) and $F_X/F_{opt} = 0.01$ (Fischer et al. 1999), AE For is a prominent member of this group. In the catalogue of Szczygieł et al. (2008) it is one of the closest X-ray active binaries, whose L_X/L_{opt} ratio reaches 0.01 (Fischer et al. 1999). An X-ray flaring activity of the system was reported by Fuhrmeister & Schmitt (2003). It is also a bright IR source, with 2MASS magnitudes $J = 7.52$, $H = 6.85$ and $K = 6.66$.

For about a decade it has been known that active dwarfs of K and M type tend to be larger and cooler than the theory predicts. While possible solutions of this problem have been proposed (see e.g. Morales, Ribas & Jordi 2008 and references therein), it is certainly worthwhile to enlarge the relevant observational databasis. The best opportunity for this is offered by detached binaries on the lower main sequence, which allow to determine masses and radii of their components with an accuracy better than 1 per cent. AE For is clearly one of such systems, however until very recently neither the light curve nor the velocity curve of this potentially interesting binary has been studied. A preliminary light-curve solution has been derived by ZSU, who concluded that a spectroscopic analysis was needed to confirm the physical parameters of the components to a higher accuracy.

In the present paper we obtain and analyze the velocity curve of AE For, and refine the photometric solution of ZSU based on additional observations. The photometric and spectroscopic data are described in Sects. 2 and 3. The

⋆ Based in part on data obtained at the Las Campanas Observatory.

† E-mail: mnr@camk.edu.pl

Table 1. List of light curves used in this paper for photometric solutions of AE For.

1^{st} day [HJD-2400000]	last day	Filter	Number of data points	Ref.
55174	55184	Johnson B	160	1
55174	55184	Johnson V	482	1
55568	55578	Johnson B	173	2
55568	55578	Johnson V	175	2
55568	55578	Cousins R	173	2

1: our own data; 2: Zasche et al. (2012).

analysis of the data is detailed in Sect. 4, and its results are discussed in Sect. 5.

2 PHOTOMETRIC OBSERVATIONS

The observational material consists of our own BV data and BVR data of ZSU (see Table 1 for details). Our data were collected during 11 nights between 2009 Dec 8/9 and Dec 18/19 with the 1-m Swope telescope at Las Campanas Observatory (LCO), Chile. All the nights were clear, with the seeing between 1.1 and 2.5 arcsec. AE For was monitored with the 2048×3150 pixel SITe3 CCD camera at a scale of 0.435 arcsec/pixel. We collected 482 frames through the V filter with exposure times 5-10 s (depending on the seeing), and 160 frames in the B filter with exposure times 8-25 s. All images were de-biased and flat-fielded within the IRAF[1]

For photometric measurements the Daophot package (Stetson 1987) was employed, and differential aperture photometry was extracted using two stars in the vicinity of AE For. On every night AE For was observed we also observed NGC 2204. For six red clump stars of the latter we found the offset between instrumental magnitudes and the standard BV magnitudes determined by Rozyczka et al. (2007). Using that offset together with the average extinction for LCO ($k_V = 0.14$ and $k_B = 0.24$; see Mininti, Claria & Gomez 1989), and accounting for a 0.04 difference in air-mass between AE For and NGC 2204, we transformed the instrumental light curves of the variable to the standard BV system. Color terms of the transformation were accounted for. We estimate the error of this transformation at ± 0.02 mag, its main source being the uncertainty of the zero-point for NGC 2204. The formal error of the differential photometry is about ten times smaller.

The last three rows in Table 1 refer to BVR measurements performed by ZSU in January 2011 at the South African Astronomical Observatory, (their data are accessible online at http://vizier.cfa.harvard.edu/viz-bin/VizieR?-source=J/A+A/537/A109). Accessible online were also Hipparcos (ESA 1997), ASAS (Pojmanski 2002), and Pi of the Sky (Burd et al. 2005) light curves. However, their quality was too poor to use them for photometric solutions.

Based on almost 70 primary and secondary minima observed by various authors, ZSU derived the following ephemeris of AE For:

$$HJD_{\rm min} = 2452605.97070(35) + 0.91820943(12) \times E \qquad (1)$$

The final light curves obtained from the data collected at LCO and phased with this ephemeris are shown in Fig. 1. Evident is a strong asymmetry, which we attribute to the activity of the system, manifesting itself by large spot(s) on at least one of the components (see also Sects. 3 and 4). For the short flat part of the V-curve which begins right after the secondary eclipse (see Fig. 1) we obtained $V = 10.27 \pm 0.02$ mag. To within the errors, our $(B-V)$ index was constant throughout the orbital period, and equal to 1.35 ± 0.03 mag. For the same part of the light curve the online data of ZSU yield $V = 10.23 \pm 0.01$ mag and $(B-V) = 1.34 \pm 0.02$ mag. Marginal differences between our results and theirs may be due to the spot-related variability of at least one component of AE For.

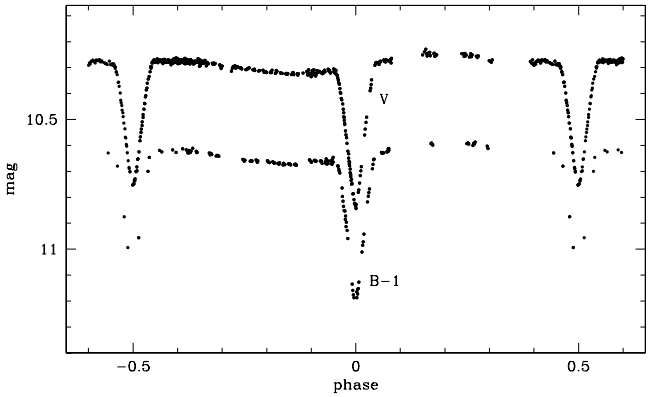

Figure 1. Light curves of AE For obtained in December 2009 at Las Campanas Observatory. To save the plotting space the B-curve is shifted upward by one magnitude.

3 SPECTROSCOPIC OBSERVATIONS

The spectroscopic data were collected with the Echelle Spectrograph on the 2.5-m Irénée du Pont telescope at LCO. The spectrograph, equipped with the SITe2K CCD camera, was working at a slit width of 1.0 arcsec, providing a resolution of ∼45,000. The observations were performed in two runs: four nights from 2009 Nov 23/24 to Nov 26/27 and five nights from 2010 Dec 19/20 to Dec 23/24. All the nights were clear but a half of one night with thin cirrus clouds. For most (∼90 per cent) exposures the airmass was smaller than 1.4. During the observations pairs of 480-s exposures of the scientific target were made, interlaced with a 90-s exposure of a ThAr lamp spectrum.

The observations were reduced within the IRAF ECHELLE package. After bias and flat-field correction, each pair of the frames was combined into a single frame, allowing for the rejection of cosmic ray hits. Altogether, 31 reduced spectra were obtained, extending from ∼4000 to ∼7000 Å. All of them showed strong Balmer emission lines, and in nearly all of them the NaI doublet at 5890 and 5896 Å was

[1] IRAF is distributed by the National Optical Astronomy Observatories, which are operated by the AURA, Inc., under cooperative agreement with the NSF.

Table 2. Barycentric radial velocities of AE For phased according to the ephemeris given by equation (1).

HJD-2455000	$v_{\rm p}$ [km s^{-1}]	$v_{\rm s}$ [km s^{-1}]	phase
159.57213	9.88	110.40	0.06644
159.63862	-28.91	148.95	0.13885
159.70775	-52.93	177.94	0.21414
159.77389	-53.68	175.07	0.28617
159.78416	-51.58	173.19	0.29736
160.52630	-14.47	134.61	0.10560
160.62988	-53.98	175.83	0.21841
160.64699	-56.77	179.20	0.23704
160.67158	-57.13	179.58	0.26382
160.75599	-30.58	151.97	0.35575
161.61738	-52.80	174.11	0.29387
161.73443	3.17	117.71	0.42135
162.53278	-53.57	174.34	0.29081
162.54966	-49.00	170.00	0.30920
162.60757	-24.52	145.63	0.37227
162.64129	-5.39	126.63	0.40899
162.81241	126.34	-7.49	-0.40465
162.82922	138.43	-20.31	-0.38634
550.55538	143.22	-24.08	-0.12303
550.57283	129.29	-10.95	-0.10402
550.58045	124.95	-6.27	-0.09573
551.73601	-38.74	161.16	0.16277
551.75427	-47.05	168.90	0.18265
552.68821	-50.75	173.13	0.19979
552.70336	-54.04	175.98	0.21629
552.71858	-56.71	178.77	0.23286
553.59737	-49.76	170.50	0.18993
553.67500	-54.54	177.94	0.27448
553.73276	-39.80	162.90	0.33738
554.61505	-50.65	172.56	0.29827
554.67243	-27.41	150.57	0.36076

blended into a very broad (∼15 Å, or ∼760 km s^{-1}) absorption feature.

Radial velocities were measured using an implementation of the broadening function formalism (Rucinski 2002) described by Kaluzny et al. (2006).[2] Since including emission lines or broad absorption features would decrease the accuracy of velocity measurements, a wavelength range devoid of such features had to be selected. Shortward of H_γ the spectra were too noisy, so that our choice was reduced to four segments limited by H_γ H_β, NaI doublet, H_α and O_2 b-band. We chose the segment between H_β and NaI doublet, extending from 4870 to 5845 Å. It was the longest one of the four, and the only one in which the mean S/N ratio was larger than 20 for all the spectra. The solar-scaled synthetic spectrum for $T = 4000$ K and $\log g = 5.0$ from the library of Coelho et al. (2005) served as a template.

The observed velocity curve was fitted with a nonlinear least-squares solution, using a spectroscopic data solver written and kindly provided by Guillermo Torres. Because to within observational errors secondary minima are separated from the primary ones by half the period, a circular orbit was assumed, and the eccentricity e was fixed at 0 (the same assumption was adopted by ZSU). The resulting barycentric

[2] The software package used in this paper is freely accessible at http://users.camk.edu.pl/pych/BF/.

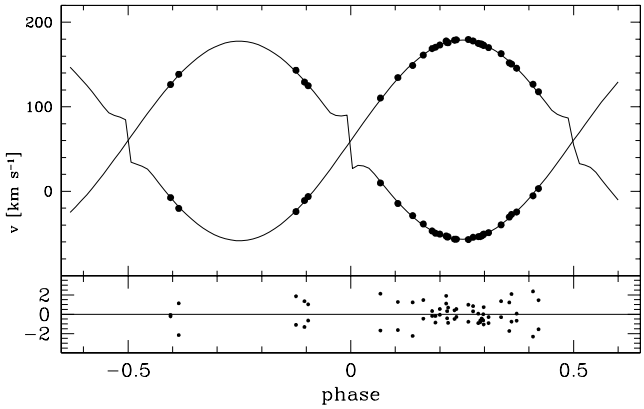

Figure 2. Velocity curve of AE For based on the data contained in Table 2. The rms residual velocity calculated from all (i.e. primary's and secondary's) residua shown in the bottom panel is equal to 1.13 km s^{-1}. Phase 0 corresponds to the center of the primary photometric minimum.

radial velocities are listed in Table 2 and plotted in the upper panel of Fig. 2 together with the fitted velocity curve. The mean error of velocity measurement, estimated from the residual velocities shown in the bottom panel of Fig. 2, is ±1.13 km s^{-1}. Its rather large value may result from line blending and/or asymmetries (the latter being caused by large spots; see also Sects. 2 and 4). We repeated the measurements using a synthetic spectrum for $T = 4250$ K to find that the changes in the observed velocities were much smaller than the scatter of points around the fit. We also tried out the remaining three wavelength ranges, however in all cases the fit had a lower quality (i.e. the residual velocities were larger).

The derived orbital parameters are listed in Table 3 together with formal 1-σ errors returned by the fitting routine. Note that, despite the rather large residual velocities, the solution is fairly accurate - relative errors in $M \sin^3 i$ and $A \sin i$ amount to 0.5 and 0.15 per cent, respectively.

4 LIGHT CURVE ANALYSIS AND SYSTEM PARAMETERS

The analysis of the light curves was performed with the PHOEBE implementation (Prša & Zwitter 2005) of the Wilson-Devinney (WD) model (Wilson & Devinney 1971; Wilson 1979). The PHOEBE/WD package utilizes the Roche geometry to approximate the shapes of the stars, uses Kurucz model atmospheres, treats reflection effects in detail, and, most importantly, allows for the simultaneous analysis of B and V data. Appropriately for stars with convective envelopes, we adopted gravity darkening coefficients $g_p = g_s = 0.32$ and bolometric albedos $A_p = A_s = 0.5$. The effects of reflection were included, and a logarithmic limb-darkening based on tables by van Hamme (1993) was used as implemented in PHOEBE 031a. Following ZSU, full synchronization of both components was assumed.

ZSU fitted the light curves of AE For with the help of the program ROCHE (Pribulla 2004). Keeping in mind that

Table 3. Orbital parameters

Parameter	Unit	Value
γ	km s^{-1}	59.95±0.23
K_p	km s^{-1}	116.92±0.33
K_s	km s^{-1}	119.12±0.33
e		0.0[a]
σ_p	km s^{-1}	1.08
σ_s	km s^{-1}	1.18
Derived quantities:		
$A \sin i$	$R_\odot$	4.2820±0.0069
$M_p \sin^3 i$	$M_\odot$	0.6314±0.0034
$M_s \sin^3 i$	$M_\odot$	0.6197±0.0033

[a]Assumed in fit

Table 4. Photometric parameters derived from ZSU data. The lower bounds for component masses derived from the orbital solutions are 0.6314±0.0034 and 0.6197±0.0033 $M_\odot$, respectively, for the primary and the secondary.

Parameter	Unit	Original ZSU	Our fit	Our fit with spots	Dark pole
1	2	3	4	5	6
i	deg	86.51(31)	86.84	86.71	85.47
T_s	K	4065(48)	4083	4052	4041
R_p	$R_\odot$	0.66(10)	0.71	0.71	0.661
R_s	$R_\odot$	0.52(8)	0.53	0.52	0.605
$(L_p)_V$	%	63.1(1.2)	65.4	66.8	57.2
$(L_p)_B$	%	63.2(1.3)	65.6	67.3	57.9
σ_V	mmag	17	13	12	13

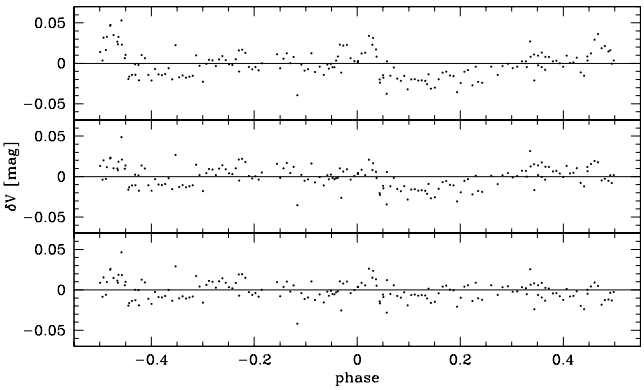

Figure 3. Residuals of fits listed in columns 3–5 of Table 4. Top: original ZSU: middle: PHOEBE-iterated starting from ZSU parameters, bottom: same as middle, but with spots added on both components (see text for details).

their ROCHE and PHOEBE fits of GK Boo were markedly different (although not at a statistically significant level), we decided to check if our photometric solution of AE For will be compatible with theirs. We fed their photometric data into PHOEBE, and iterated upon inclination i, secondary's temperature T_s, primary's radius R_p and secondary's radius R_s, using values obtained by ZSU as initial values. The mass ratio q was fixed at a value of 0.98522 calculated from Table 3, and the orbital separation A – at 4.28996 $R_\odot$ obtained from $A \sin i$ in Table 3 for the inclination $i = 85.51°$ found by ZSU. Following ZSU, we kept the temperature of the primary T_p fixed at 4100 K. To within the errors, this value agrees with 4055±71 K resulting from the $T_{eff} - (B - V)$ calibration of Ramirez & Melendez (2005), and marginally agrees with 4005±92 K resulting from the analogous calibration of Worthey & Lee (2011). The latter two values, however, should be treated with some caution, since AE For emits most energy in the near-IR range beyond B and V passbands, at 2MASS magnitudes $J = 7.52$, $H = 6.85$ and $K = 6.66$. An infrared calibration would be more appropriate; unfortunately we have not found any such relation extending up to $(J - K) = 0.86$. The problem of the temperature is further discussed in Sect. 5.

The results of fitting are listed in columns 3 and 4 of Table 4. Column 3 contains the original values obtained by ZSU together with their errors. The corresponding synthetic light curves produced by PHOEBE without any iterations turned out to be fairly well fitting, with a standard deviation of V-residuals equal to 17 mmag (similar values were obtained for B and R bands). The iterations improved the quality of the fit (σ_V was reduced to 13 mmag), but the parameters did not change in a statistically significant way (column 4). We performed an additional iteration with the following spots introduced on both components at a latitude of 90° (i.e. at the equator in PHOEBE's convention): one on the primary at a longitude of 180° with a radius of 20° and temperature factor of 0.98; two on the secondary at longitudes = 125° and 330°, both of them with a radius of 30° and temperature factor of 1.02. The residuals became more symmetric (see Fig. 3) and σ_V was reduced to 12 mmag, but no statistically significant corrections to system parameters were obtained (column 5 of Table 4). We note that by "spot" we mean a fairly large region on the surface of a star, whose mean temperature is elevated or reduced due to an excess of genuine stellar spots with much smaller sizes.

For the assumed $M_s = 0.5M_\odot$, ZSU derived $R_s = 0.52R_\odot$, and our PHOEBE iterations confirmed this result. However, while a radius of $0.52R_\odot$ may be compatible with the mass of $M_s = 0.5M_\odot$ assumed by ZSU, it is excluded by our spectroscopic solution, in which $M_s > 0.6M_\odot$. This is because within a broad range of metallicity ($-0.5 \leqslant$ [Fe/H] $\leqslant 0.5$) and α-enhancement ($-0.2 \leqslant$ [α/Fe] $\leqslant 0.4$) a main-sequence star with M=$0.6M_\odot$ never becomes that small (see Dotter et al. 2008, and the DSED evolutionary tracks at http://stellar.dartmouth.edu/models/index.htm). Another argument in favor of a larger secondary is based on rotational velocity fits which are performed automatically within the BF formalism during radial velocity measurements. Upon averaging velocities fitted in 2009 and 2010 we got $v_{\mathrm{rot},s} = 37.46$±2.40 km s^{-1} for the primary and $v_{\mathrm{rot},s} = 37.07$±2.20 km s^{-1} for the secondary. For the assumed synchronous rotation these values imply $R_p = 0.680 \pm 0.044R_\odot$ and $R_s = 0.673 \pm 0.040R_\odot$.

The simplest way to remove this contradiction is to force a smaller inclination i: one may expect that R_s will then increase, so that depths and widths of the minima are preserved. This may be achieved, for example, by placing a dark spot around the uneclipsed pole of the primary. We performed an experiment, in which the circumpolar region of the primary with a radius of 50° had a temperature factor of 0.95. As shown in column 6 of Table 4, the iterations yielded a solution with i smaller by more than one degree and R_s

Table 5. Photometric parameters derived from our data

Parameter	Unit	P0 S0	P0 S1h2c	P1h S2c	P1c S1h1c	Mean col. 4-6
1	2	3	4	5	6	7
i	deg	85.72	85.75	85.51	85.43	85.6±0.2
T_s	K	4016	4055	4061	4050	4055±6
R_p	$R_\odot$	0.705	0.694	0.665	0.650	0.67±0.03
R_s	$R_\odot$	0.603	0.607	0.640	0.654	0.63±0.03
$(L_p)_V$	%	61.6	58.8	53.8	52.1	54.9±4.4
$(L_p)_B$	%	62.5	59.4	54.2	52.7	55.4±4.4
σ_V	mmag	20.1	7.0	6.5	6.5	–

Table 6. Parameters of spots for models from Table 5

Model	component	latitude	radius	temp.factor
P0S1h2c	S	60	40	0.99
	S	100	30	1.02
	S	230	30	0.95
P1hS2c	P	280	30	1.02
	S	60	40	0.99
	S	230	30	0.95
P1cS1h1c	P	240	40	0.99
	S	100	30	1.02
	S	230	30	0.95

larger by almost 0.1 $R_\odot$ compared to the model without a darkened pole.

At this point we faced the problem whether to include clearly unphysical solutions in final estimates of system parameters, and we decided to reject them. Apparently, ZSU collected their data when the system was in a particular state making the analysis very uncertain, and to remain on the safe side we calculated the parameters of AE For based on our photometry only.

Photometric solutions based on our own data are listed in Table 5. Four models are shown, identified by the numbers of hot (h) and cold (c) spots on the primary (P) and the secondary (S). In each spotted model there are three spots centered at a latitude of 90°. The remaining parameters of the spots are listed in Table 6. The fit without spots (P0S0) is poor, as indicated by a large σ_V. Its low quality is clearly seen in Fig. 4, in which the residuals show systematic deviations with an amplitude exceeding 40 mmag. Introducing spots makes the fit nearly ideal. Not surprisingly, however, Table 5 shows that different spot arrangements result in different system parameters. The encouraging finding is that for all models (even for the unspotted one) the inclination angle is by about one degree smaller than that obtained from ZSU data, and the radius of the secondary is consistently larger than $0.6R_\odot$. The last column of Table 5 contains averaged values of spotted model parameters together with formally calculated errors. Since the distribution of spot-dependent model parameters is most probably non-Gaussian, these errors should be treated with caution, and we give them only to approximately illustrate the uncertainties resulting from the nonexistence of a unique configuration of spots.

Independently of their spot-related uncertainty, the models have Gaussian errors related to nonzero residuals,

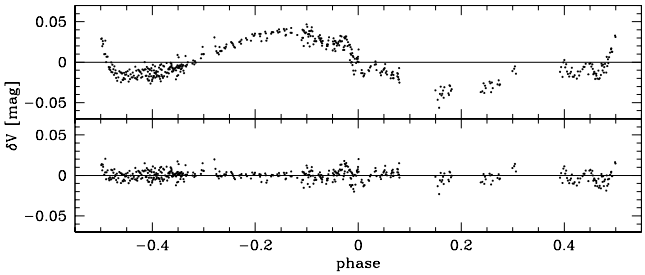

Figure 4. Residuals of fits listed in columns 3 and 4 of Table 5. Top: model P0S0 (without spots); bottom: model P0S1h2c (three spots on the secondary; see Table 6 for details).

which we estimated using a Monte Carlo procedure written in PHOEBE-scripter. Briefly, the procedure replaces the observed light curves B_{obs} and V_{obs} with the fitted ones B_f and V_f, generates 20000 Gaussian perturbations δB_f and δV_f such that the standard deviation of each of them is equal to the standard deviation of the residuals $B_f - B_{obs}$ or $V_f - V_{obs}$, and for each perturbation performs PHOEBE iterations on $V_f + \delta V_f$ and $B_f + \delta B_f$. In all cases the Gaussian errors turned out to be much smaller than the formal errors of averaged parameters given in column 7 of Table 5.

The final absolute parameters of AE For are given in Table 7 (bolometric magnitudes in the last two rows are averages of the values taken directly from PHOEBE output). The errors of A, M_p and M_s include the inclination uncertainty. As we explained above, the errors of the remaining parameters are but an approximate illustration of the uncertainties related to the presence of spots.

5 DISCUSSION AND CONCLUSIONS

The fits described in Sect. 4 indicate that an unavoidable consequence of spot activity is the degradation of the photometric solution: based on the available data, the radii of the components cannot be calculated with an accuracy better than ∼5 per cent. As we have shown in Sect. 4, the asymmetric and highly variable light curve of AE For can even generate nonphysical solutions in which one of the stars is unrealistically small. The only way to improve the accuracy of system parameters is via collecting more photometric data from various seasons and careful fitting of each light curve with various arrangements of spots (see e.g. Rozyczka et al. 2009). Alternatively, many light curves from various seasons might be averaged in hope that the mean curve would be free from spot-caused irregularities.

Another potential source of uncertainties in our final parameters is the effective temperature of the primary, which we fixed at 4100 K (i.e. a value adopted by ZSU). Luckily, the temperature only weakly affects i, R_s and R_p – we checked that they all change by less than 0.2 per cent for a ±150 K change in T_p. It is thus possible to compare the derived radii with stellar models, and such a comparison with the synthetic main sequence represented by the 1 Gyr Dartmouth isochrone for [Fe/H] = 0.0 and [α/Fe] = 0.0 is shown in Fig. 5. Each component of AE For is clearly oversized vs. a main-sequence star of the same mass. This conclusion holds for a broad range of chemical composition parameters ($-0.5 \leqslant$ [Fe/H] $\leqslant 0.5$; $-0.2 \leqslant$ [α/Fe] $\leqslant 0.4$).

Table 7. Absolute parameters of AE For

Parameter	Unit	Value
A	$R_\odot$	4.2820±0.0069
i	deg	85.6 ±0.2[a]
e		0[b]
M_p	$M_\odot$	0.6314±0.0035
M_s	$M_\odot$	0.6197±0.0034
R_p	$R_\odot$	0.67±0.03[a]
R_s	$R_\odot$	0.63±0.03[a]
T_p	K	4100[b]
T_s	K	4055±6[a]
M_p^{bol}	mag	7.15±0.09[a]
M_s^{bol}	mag	7.32±0.11[a]

[a]Approximate errors due to spots (see text)
[b]Assumed in fit

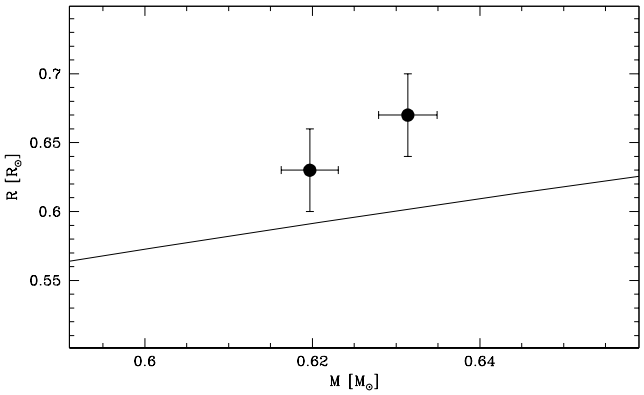

Figure 5. Location of our final solution in the $(M-R)$ plane. Solid line: main sequence represented by the 1 Gyr Dartmouth isochrone for solar abundances.

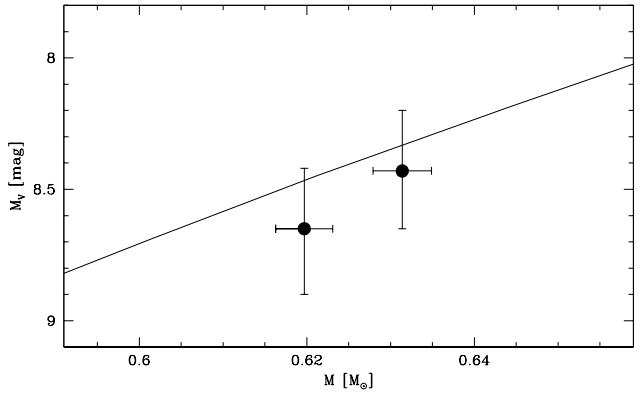

Figure 6. Location of AE For components in the $(M-M_V)$ plane. The magnitudes are derived from the observational data. Solid line: the same isochrone as in Fig. 5.

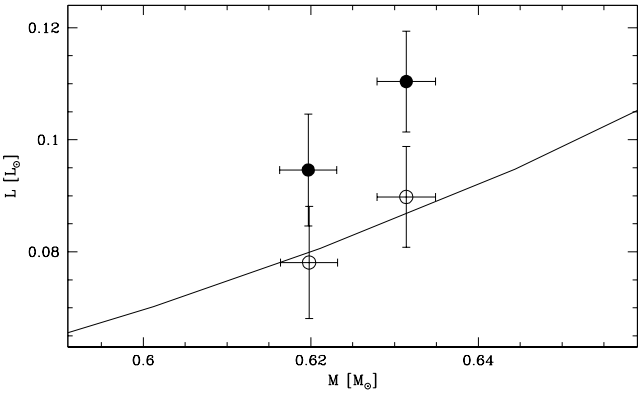

Figure 7. Location of our solutions in the $(M-L)$ plane. Models with $T_p = 4100$ and $T_P = 3900$ K are identified by filled and open circles, respectively. Solid line: the same isochrone as in Fig. 5.

While active components of eclipsing binaries appear to be larger and cooler than inactive single stars of the same mass, they have a similar luminosity (Morales et al. 2008). To check if this holds for our binary, we calculated absolute magnitudes of the components in V-band from the observed magnitude and parallax of the system, using the contribution of the primary to the total light from Table 7. The location of the components in the $(M-M_V)$ plane is shown in Fig. 6 together with the main sequence represented as before by the 1 Gyr Dartmouth isochrone for solar abundances. As one can see, to within the errors both stars do indeed belong to the main sequence. In the following we assume that they have main-sequence luminosities, and based on that assumption we estimate their temperatures.

Fig. 7 indicates that the solution with $T_p = 4100$ K is significantly too luminous. Only at $T_p = 3900$ K (for which $T_s = 3860$ K) do both stars align with the main sequence, suggesting that the temperature assumed by ZSU and the temperatures derived from the calibrations of Ramirez & Melendez (2005) and Worthey & Lee (2011) are overestimated. Of course, this finding should be verified, preferably by using disentangling software (see e.g. Hadrava 2009). Further spectroscopic observations are needed for that purpose, collected during low-activity periods. When the system is active, all temperature estimates, whether based on spectral fitting or photometric calibrations, are likely to be flawed because of large spotted areas present on both components.

We have thus proved the consistency of the assumption that the components of AE For are main-sequence stars. However, given the large errors of M_V, a possibility that they have not yet settled on the main sequence should also be explored. If they were indeed in the contraction phase, their large sizes could be at least partly caused by evolutionary effects. Such a possibility is indicated by the Li 6708 Å line identified in the spectrum of AE For by Torres et al. (2006). With an equivalent width of 80 mÅ it falls right in the middle of the range observed for Pleiades members with the same $(V-I)$, suggesting that the system is rather young. Unfortunately, our efforts to repeat the measurement of Torres et al. (2006) were unsuccessful. We do not claim that the line is not there: our spectra may be too noisy, or the broadening is too strong, or both. It is worth mentioning, however, that based on kinematic criteria, Eggen (1990) assigned AE For to the Hyades supercluster whose age is estimated at ∼0.6 Gyr (Montes et al. 2001). If this assignment is correct, then both components of the binary must have ended their pre-main sequence evolutionary phase long ago. Again, high-quality spectra, collected preferably during eclipses, are needed to resolve the Lithium (and age) problem.

Yet another explanation for the oversized components involves the third body discovered by ZSU. In a triple system consisting of a binary orbited by a distant companion both the eccentricity of the binary e_b and the inclination of the third body's orbit execute periodic Kozai oscillations. If at some phase of the oscillation cycle e_b becomes sufficiently large for tidal friction to dissipate the orbital energy of the binary, then the binary gradually tightens its orbit (see e.g. Fabrycky & Tremaine 2007, and references therein). The associated tidal heating could temporarily inflate the components; however, since nearly all close binaries are members of triple systems (Tokovinin et al. 2006), and the inflation effect is limited to low-mass stars of K and M type (Morales et al. 2008), we consider this explanation much less likely than the remaining two (especially than that related to stellar activity).

The above discussion indicates that AE For is a truly interesting object which clearly deserves closer attention. A systematic study of this system would certainly bring valuable information concerning the activity of late-type stars.

ACKNOWLEDGMENTS

We are greatful to the anonymous referee for the detailed and helpful report. Support for R.A. is provided by Proyecto GEMINI CONICYT #32100022 and via a Postdoctoral Fellowship by the School of Engineering at Pontificia Universidad Católica de Chile. Support for I.D. is provided by the Chilean Ministry for the Economy, Development, and Tourisms Programa Inicativa Científica Milenio through grant P07-021-F, awarded to The Milky Way Millennium Nucleus, and by Proyecto FONDECYT Regular #1110326. We thank Guillermo Torres for providing the spectroscopic data solver. This research has made use of the SIMBAD database, operated at CDS, Strasbourg, France.

REFERENCES

Burd A. et al., 2005, NewA, 10, 409
Coelho P., Barbuy B. J., Meléndez J., Schiavon R. P., Castilho B. V., 2005, A&A, 443, 735
Dotter A., Chaboyer B., Jevremović D., Kostov V., Baron E., Ferguson J. W., 2008, ApJS, 178, 89
Eggen O. J., 1990, PASP, 102, 166
ESA, 1997, The Hipparcos and Tycho Catalogues, ESA SP-1200
Fabrycky D. & Tremaine S., 2007, ApJ, 669, 1298
Fischer J.-U., Hasinger G., Schwope A. D., Brunner H., Boller T., Trümper J., Voges W., Neizvestnyj S., 1998, Astron. Nachr., 319, 347
Fuhrmeister B., Schmitt J. H. M. M., 2003, A&A, 403, 247
Gizis J. E., Reid I. N., Hawley S. L., 2002, AJ, 123, 3356
Gray R. O., Corbally C. J., Garrison R. F., McFadden M. T., Bubar E. J., McGahee C. E., O'Donoghue A. A., Knox E. R., 2006, AJ, 132, 161
Hadrava P., 2009, A&A, 494, 399
Huensch M., Schmidt J. H. M. M., Sterzik, F. F., Voges, W., 1999, A&A Suppl., 135, 319
Kaluzny J., Pych W., Rucinski S. M., Thompson I. B., 2006, AcA, 56, 237
Minniti D., Claria J. J., Gomez M. N., 1989, Ap&SS, 158, 9
Montes D.; López-Santiago J., Gálvez M. C., Fernández-Figueroa M. J., De Castro E., Cornide M., 2001, MNRAS, 328, 45
Morales J. C., Ribas I., Jordi C., 2008, A&A, 478, 507
Pojmanski G., 2002, AcA, 52, 397
Pribulla T., 2004, Spectroscopically and Spatially Resolving the Components of the Close Binary Stars, ASP Conf. Ser. 318, 117S
Prša A., Zwitter T., 2005, ApJ, 628, 426
Ramírez I., Melendez J., 2005, ApJ, 626, 465
Rozyczka M., Kaluzny J., Krzeminski W., Mazur B., 2007, AcA 57, 323
Rozyczka M., Kaluzny J., Pietrukowicz P., Pych W., Mazur B., Catelan M., Thompson I. B., 2009, AcA 59, 385
Rucinski S. M., 2002, AJ, 124, 1746
Stephenson C. B., 1986, AJ, 92, 139
Stetson P. B., 1987, PASP, 99, 191
Szczygieł D. M., Socrates A., Paczyński B., Pojmanski G., Pilecki B., 2008, AcA 58, 405
Tokovinin A., Thomas S., Sterzik M., & Udry S., 2006, A&A, 450, 681.
Torres C. A. O., Quast G. R., da Silva L., de La Reza R., Melo C. H. F., Sterzik M., 2006, A&A, 460, 695
van Hamme W., 1993, AJ, 106, 2096
van Leeuwen F., 2007, Hipparcos, the new reduction of the raw data, ASSL 350, Springer 2007
Wilson R. E., 1971, ApJ, 234, 1054
Wilson R. E., Devinney E. J., 1971, AJ, 166, 605
Worthey G., Lee H-C., 1971, AJ, 166, 605
Zasche P., Svoboda P., Uhlář R., 2012, A&A, 537, A109 (ZSU)

Table 8. A sample of the B-lightcurve of AE For.

HJD-240000	B [mag]
55174.610258	11.629
55174.629343	11.680
55174.650730	11.994
55174.673195	11.956
55174.695058	11.646
55174.715983	11.619

Table 9. A sample of the V-lightcurve of AE For.

HJD-240000	V [mag]
55174.662443	10.745
55175.581451	10.744
55174.664191	10.731
55175.583256	10.733
55174.665765	10.725
55174.667675	10.697

ONLINE MATERIAL